Journal of Power Sources 273 (2015) 754–760

Contents lists available at ScienceDirect

Journal of Power Sources

journal homepage: www.elsevier.com/locate/jpowsour

Graphene oxide/lithium titanate composite with binder-free as high capacity anode material for lithium-ion batteries

Zhengwei Xie [a, b], Xiang Li [a, b], Wen Li [a, b], Mianzhong Chen [a], Meizhen Qu [a, *]

[a] Chengdu Institute of Organic Chemistry, Chinese Academy of Sciences, Chengdu 610041, PR China
[b] Graduate University of Chinese Academy of Sciences, Beijing 100039, PR China

HIGHLIGHTS

- LTO particles well dispersed among graphene oxide nanosheets.
- Graphene oxide can replace the polymer binder.
- LGC-10% electrode has a higher reversible Li-storage specific capacity.
- LGC-10% electrode exhibits an excellent rate and cycling performance.

GRAPHICAL ABSTRACT

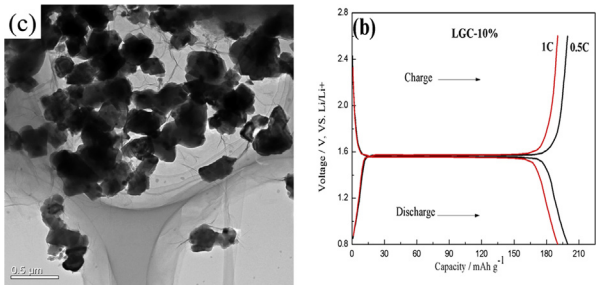

ARTICLE INFO

Article history:
Received 9 August 2014
Received in revised form
22 September 2014
Accepted 24 September 2014
Available online 2 October 2014

Keywords:
Graphene oxide
Lithium titanate
Capacity
Rate
Binder-free

ABSTRACT

A series of composites of $Li_4Ti_5O_{12}$ particles well dispersed among graphene oxide (GO) nanosheets as binder-free anode materials for high capacity and rate lithium-ion batteries are prepared and investigated. The morphology, microstructure and elemental compositions of the as-prepared composites are characterized by scanning electron microscopy, transmission electron microscopy, X-ray diffraction and X-ray photoelectron spectroscopy. Electrochemical tests reveal that the electrode with GO content 10% presents a reversible Li-ion storage specific capacity of 201 mAh g^{-1} at 0.5C (1C = 175 mA g^{-1}), and the specific capacity still maintain in 162 mAh g^{-1} even at 30C. Moreover, this composite exhibits an excellent cycling stability, with a first charge capacity of 162 mAh g^{-1} at 30C and less than 3% loss after 300 cycles. The addition of GO provides the additional capacity via oxygen-containing functional group and nano-cavity, additionally, replacing the CMC by GO, which makes the composite with CMC binder-free, speeds up the lithium ion diffusion in anode materials.

1. Introduction

As one of the most promising anode materials for the application of power sources to replace graphite or carbon in electric vehicles (EV), hybrid electric vehicles (HEV) and plug-in hybrid vehicles (PHEV) [1,2], spinel $Li_4Ti_5O_{12}$ (LTO) has been investigated in recent years due to its zero volume change, no formation of solid electrolyte interphase layer and metallic lithium during discharge/charge processes, high working potential of the redox couple Ti^{4+}/Ti^{3+} (ca. 1.55 V vs. Li/Li^+), excellent safety and thermal stability [3,4]. However, the low specific capacity (175 mAh g^{-1} for theoretical and 160 mAh g^{-1} for actual) and poor intrinsic electronic conductivity of LTO, seriously hinder its large-scale application as high energy density and rate performance batteries [5].

In order to overcome the shortcomings of LTO material mentioned above, many efforts have been made, such as particle size reducing [6–9], ion doping [10–13] and carbon coating

* Corresponding author. Tel.: +86 28 85228839; fax: +86 28 85215069.
E-mail addresses: xiezhengwei116@hotmail.com (Z. Xie), mzhqu@cioc.ac.cn (M. Qu).

http://dx.doi.org/10.1016/j.jpowsour.2014.09.154
0378-7753/

[14–18], etc. Nevertheless, the actual specific capacity of LTO is hard to exceed 170 mAh g^{-1}.

As the precursor of graphene, GO has been proved to have good electrochemical performance in our previous work [19,20] such as a higher lithium storage capacity than traditional graphite and $Li_4Ti_5O_{12}$ anode materials. In addition, GO is also easy to form self-assembly membrane instead of polymer binder.

In this work, commercial LTO, GO (made in our own laboratory) and conductive carbon black were applied to fabricate LTO composites (nominated as LGC), and in these novel composites, LTO can play a great role in holding back stack of GO sheets, in stabilizing electrochemical property and providing Li-ion storage capability. GO, can not only play the role of the Li-ion storage, but also the effect of binder. So the LGC composites can be directly used as electrodes without adding any other binders, and present a very high reversible capacity.

2. Experimental

2.1. Preparation of GO and LGC composites

Commercial LTO powders (Chengdu Xingneng New Materials Co., LTD) and 4A-Zeolite (Kelong Chemical Reagent Crop. Chengdu China) were used in our study. GO was synthesized from high-purity natural flake graphite (about 200 meshes, Changsha Shenghua Research Institute, 99.999%) by a modified Hummers method [21,22]. And the colloidal dispersion of GO in deionized water was prepared with the aid of ultrasound (20 kHz ultrasound probe) treatment about 30 min to give a stable amber dispersion. Conductive additive used in the composites was Super-P carbon black (40 nm, 62 m^2 g^{-1}, TIMCAL Graphite & Carbon). The LTO slurry was prepared by mixing adequate deionized water with LTO, CMC and conductive carbon black (in a LTO/CMC/conductive carbon black weight ratio of 80:10:10) via vigorously stirring for 3 h and the LGC slurries with different proportions were prepared with the same method (in a LTO/GO/conductive carbon black weight ratio of 70:20:10, 75:15:10, 80:10:10, 85:5:10 and 87:3:10). In addition, in order to determine the influence of GO and CMC binder-free, the other two electrodes have been prepared (in a LTO/GO/CMC/conductive carbon black weight ratio of 80:5:10:5, 75:5:10:10, nominated as LGCC-1, LGCC-2, respectively).

2.2. Materials characterization

The morphology and structure of the obtained samples were determined by scanning electron microscopy (SEM; INCA Penta-FETx3) and transmission electron microscopy (TEM; JEM-100CX JEOL). Using Al/K_α radiation ($h\nu = 1486.6$ eV), X-ray photoelectron spectroscopy (XPS; PHI5600 Physical Electronics) was performed to determine elemental compositions and assignments of carbon peaks. X-ray diffraction (XRD) patterns were obtained from X'Pert MPD DY1219 using Cu/K_α radiation ($\lambda = 1.5406$ Å).

2.3. Electrochemical measurements

The working electrode was prepared as follows. First, LTO, GO dispersion (GO amount calculated according to solid content) and conductive carbon black were mixed according to the fixed proportion and ground with ethanol as solvent to form a uniform slurry, then coated onto a Cu foil and dried under vacuum at 105 °C for 12 h (the thickness and density of working electrodes are almost uniform). After the foil was cut into disks (10 mm in diameter) and pressed, coin cells were assembled with lithium metal as the counter electrode and a Celgard 2400 was employed as separator in a glove box filled with Ar gas. The electrolyte obtained from Capchem. Technology (Shenzhen) Co., Ltd. consists of a solution of 1 M $LiPF_6$ in ethylene carbonate, dimethyl carbonate, diethyl carbonate (EC/DMC/DEC, 1:1:1, in volume). Galvanostatic discharge/charge experiments were carried out on an automatic galvanostatic charge–discharge unit (Land CT 2001A, Wuhan, China) under different current densities between 0.8 and 3.0 V at 25 °C. Cyclic voltammetry (CV) and electrochemical impedance spectroscopy (EIS) tests were conducted on PARSTAT 2273 Electrochemical System (Princeton Applied Research, USA). In the case of CVs, the potential range was recorded from 0.8 to 3.0 V at different scanning rates. The EIS measurements were performed at the input signal amplitude of 10 mV (vs. open circuit potential) and the frequency ranging from 10^5 Hz to 10^{-2} Hz, and the measured data were fitted by Z-View software (Scribner Associates Inc.). All the measurements mentioned above are based on the total mass of the active material (for LTO, LTO particles is the only based material for calculation of the capacity of mAh g^{-1}, while that of the LGC electrodes include the LTO and GO).

3. Results and discussion

Fig. 1 illustrates the schematic of preparation process for LGC composites. GO and LTO are dispersed by ultrasound in alcohol to form GO dispersion and LTO suspension, respectively, and then the well-dispersed GO dispersion is added into the obtained LTO suspension. After 1 h vigorous stirring together with conductive carbon black, the mixture is heated at 70 °C to remove the solvent. Finally, a grey slurry of LGC composite is obtained. Five kinds of LGC composites (LTO/GO/conductive carbon black weight ratio of 70:20:10, 75:15:10, 80:10:10, 85:5:10 and 87:3:10) and the other two LGCC electrodes (LTO/GO/CMC/conductive carbon black weight ratio of 80:5:10:5, 75:5:10:10, nominated as LGCC-1, LGCC-2, respectively) are gained with the same method (the compositions of working electrode in detail are shown in Table 1) and tested in coin type cells. As shown in Fig. 2, the reversible charge capacity of the LTO is about 163 mAh g^{-1} at 0.5C, with the increasing of the addition of GO, the charge capacity of LGC composites increases gradually. When the content of GO is 10%, it presents the highest reversible capacity and the best cycling stability. Further increase the GO content, the capacity of LGC will begin to decline. Because when the content of GO is too much, it will be easy to stack and has lower charge capacity (Fig. S1 of Supplementary materials). However, appropriate content of GO can be separated easily by LTO particles, so the LTO and GO can play a synergy effect and show the maximum capacity. In order to express easily and intuitively, the content of GO for 10% is referred to as LGC-10%.

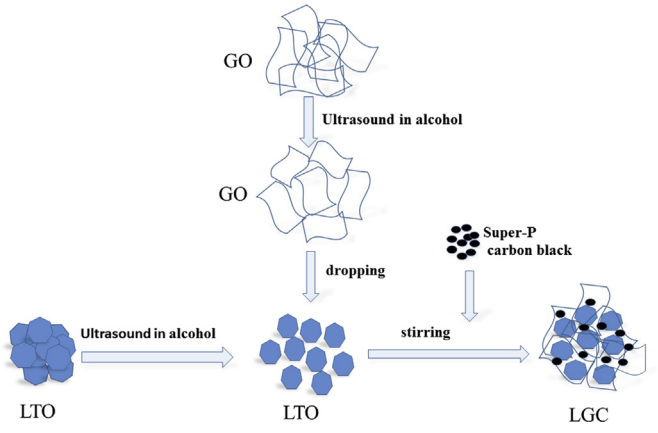

Fig. 1. Schematic of the preparation process for LGC composites.

Table 1
Summary for working electrodes composition.

Electrodes	LTO (%)	GO (%)	CMC (%)	Super P (%)
LTO	80	0	10	10
LGC-20%	70	20	0	10
LGC-15%	75	15	0	10
LGC-10%	80	10	0	10
LGC-5%	85	5	0	10
LGC-3%	87	3	0	10
LGCC-1	80	5	10	5
LGCC-2	75	5	10	10

Fig. 3 shows the XRD spectra of the LTO and LGC-10% composite. All peaks can be indexed as spinel LTO according to JCPDS File No. 49-0207 and no impurity peaks can be found. These results indicate that the addition of GO has no effect on the crystal structure of spinel LTO.

The LTO particles after ultrasonic dispersion are about 300–500 nm in size, as shown in Fig. 4a, and some of them are aggregated. From the images of the LGC-10% (Fig. 4b and c), it can be seen that the LTO particles are dispersed among the GO nanosheets, and the two dimensional (2D) wrinkled paper-like structure GO extends in all directions like a stretched network. The contact between LTO and GO can be observed from the high resolution TEM image shown in Fig. 4d. The LTO particles have a well-crystallized structure with 0.48 nm lattice spacing, consistent with the lattice spacing of (1 1 1) plane.

XPS measurement is employed to investigate the elemental compositions of the LGC-10% composite. Fig. 5a shows the XPS measurements of the LGC-10% composite. Three dominant peaks at 284.6, 286.3 and 288.1 eV are observed in C1s peak, as shown in Fig. 5b, which assign to C=C, C–O and C=O species, respectively, while the O1s peak at 529.8 eV shown in Fig. 5d is associated with Ti–O band in the LTO. Meanwhile, as shown in Fig. 5b and d, the small C1s (288.1 eV) peak as well as the small O 1s (531.3 eV) peak in the spectrum indicate the presence of oxygen-containing functional groups bonded with C atoms (such as carbonyl group) in graphene oxide nanosheets. However, the peaks of Ti–C is not observed in the C 1s and Ti 2p spectrum (Fig. 5c), which suggests no bond is formed between the LTO particles and the graphene oxide nanosheets, which also conforms to the XRD results.

Fig. 6a and b show the reversible discharge/charge curves of the LTO and LGC-10% electrodes at 0.5C and 1C. As shown in Fig. 6b, the charge capacity of the LGC-10% composite is 201 mAh g^{-1} at 0.5C,

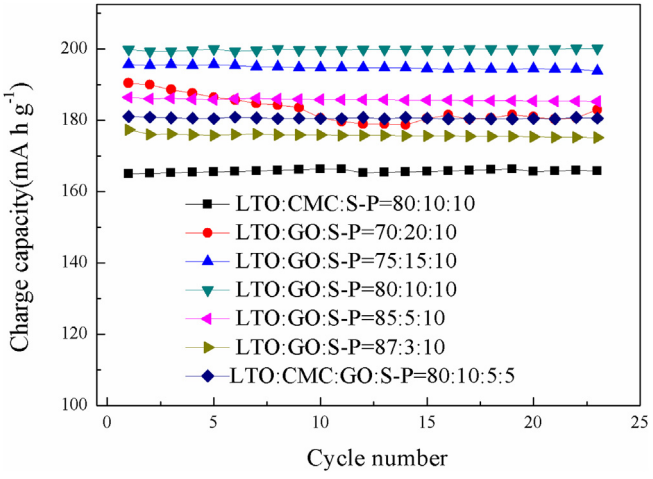

Fig. 2. Cyclic performance of LTO with different GO contents.

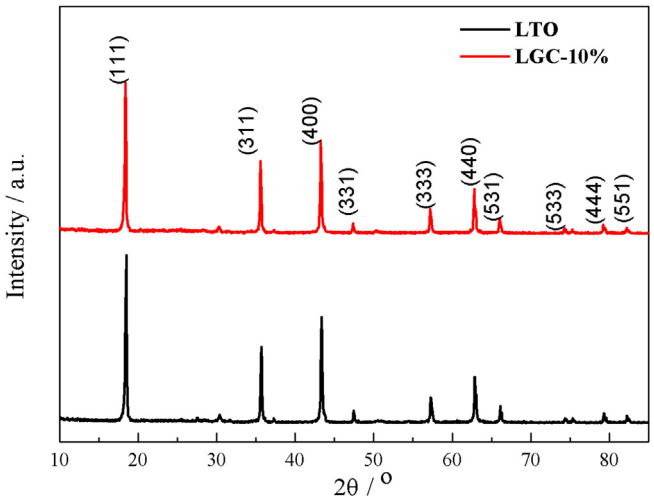

Fig. 3. XRD patterns of LTO and LGC-10% composite.

higher than the charge capacity of LTO (163 mAh g^{-1}, as shown in Fig. 6a). As far as we know, such extremely high reversible capacity at 0.5C exceeds almost all previously reported carbonaceous LTO materials, such as carbon-coated [23], graphene-coated [24,25] and so on. Obviously, this increase of reversible capacity can be attributed to GO.

In order to verify the contribution of GO to the LGC-10% composite, some experiments have been made. First of all, considering the 4A-zeolite has almost no capacity (as shown in Fig. 6c), and its particle size is similar to LTO (Fig. S2 of Supplementary materials), so together with the GO and conductive carbon black, it is adopted as the anode material to certify the role of GO. The discharge/charge test result shows that, the reversible specific capacity of 4A-Zeolite@GO (nominated as ZGC) is about 450 mAh g^{-1} and 350 mAh g^{-1} at 0.5C and 1C (as shown in Fig. 6d), which proves that the GO contributes to Li-ion storage.

The literature mentioned that Li-ion can storage in surface oxygen-containing functional groups [26]. For calculating the Li-ion storage capacity of oxygen-containing functional groups to the LGC-10%, the reduced LGC-10% (R-LGC-10%, LGC-10% reduced by hydrazine hydrate with 10 wt% carboxy-methyl cellulose (CMC) binder) is prepared. The discharge/charge test result (Fig. 6e) shows that, the reversible specific capacity of the R-LGC-10% is about 172 mAh $g^{-1}$and 162 mAh g^{-1} at 0.5C and 1C, respectively, which is close to the theoretical value (175 mAh g^{-1}) and well consistent with the corresponding literature reported [24]. Comparing to LTO, the rest of the reversible specific capacity (about 9 mAh g^{-1}, 172–163 = 9 mAh g^{-1}) may be stored in nano-cavity between LTO and GO nanosheets. The LTO, GO nanosheets and conductive carbon black particles can create some nano pores and channel, which also have the lithium ion storage capacity [27]. To verify our hypothesis, the CMC was used to block the nano pores among the LTO, GO nanosheets and conductive carbon black particles. CMC-LGC-10% electrode (C-LGC-10%, LGC-10% with 10 wt% CMC binder) is fabricated and tested, and the discharge/charge test result (Fig. 6f) illustrates that, the reversible specific capacity of the C-LGC-10% is about 191 mAh $g^{-1}$and 170 mAh g^{-1} at 0.5C and 1C, respectively, which prove that the Li-ion storage capacity of nano pores is about 10 mAh g^{-1} (201–191 = 10 mAh g^{-1}), which is accord with our hypothesis. Through the above data, we can calculate that the capacity supplied by oxygen-containing functional group and the nano pores is about 300 mAh g^{-1} and 100 mAh g^{-1}, respectively.

The LGC-10% electrode, an initial charge capacity of 201 mAh g^{-1} can be obtained at 0.5C, which is larger than that of LTO electrode,

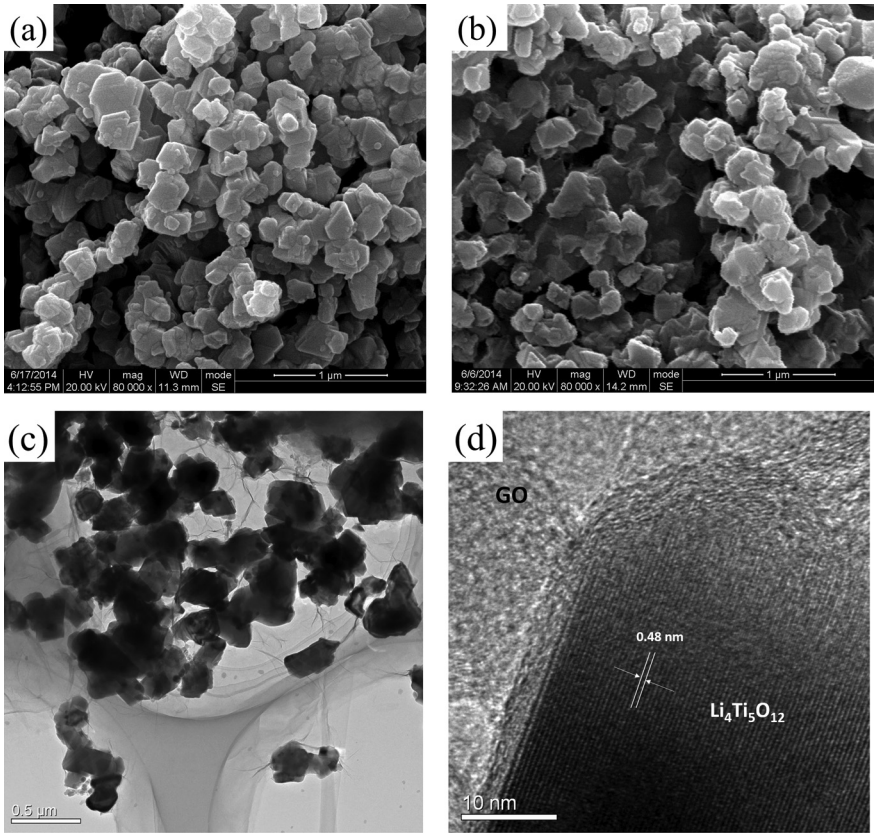

Fig. 4. SEM images of (a) LTO and (b) LGC-10% composite, and (c and d) TEM images of the LGC-10% composite at different magnifications.

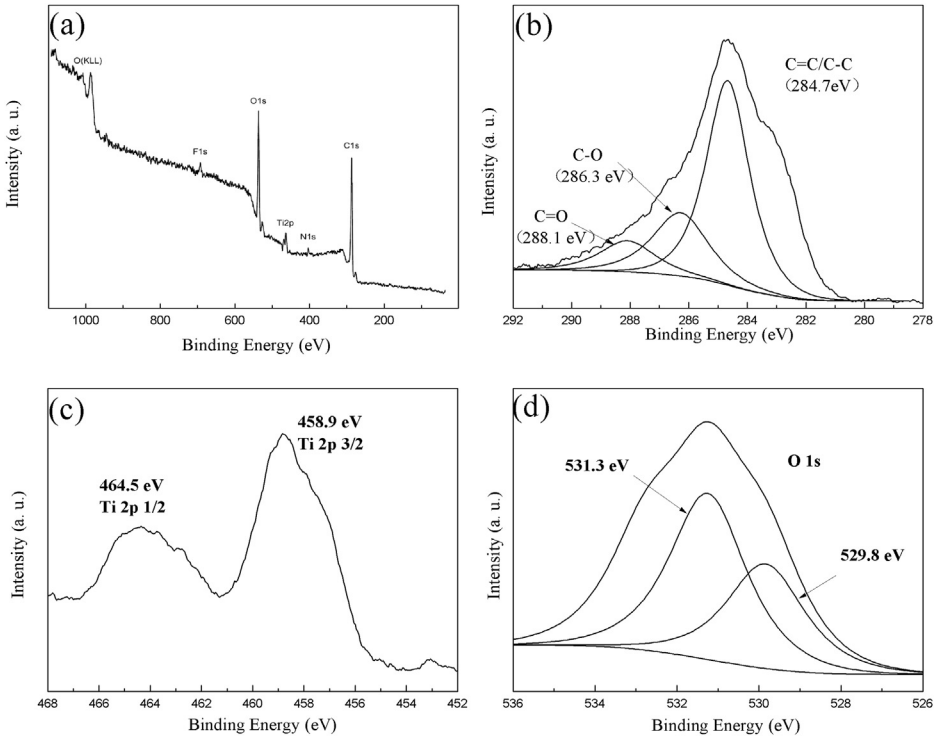

Fig. 5. (a) XPS spectra of LGC-10% electrode and (b) C 1s, (c) Ti 2p and (d) O 1s spectra of the composite.

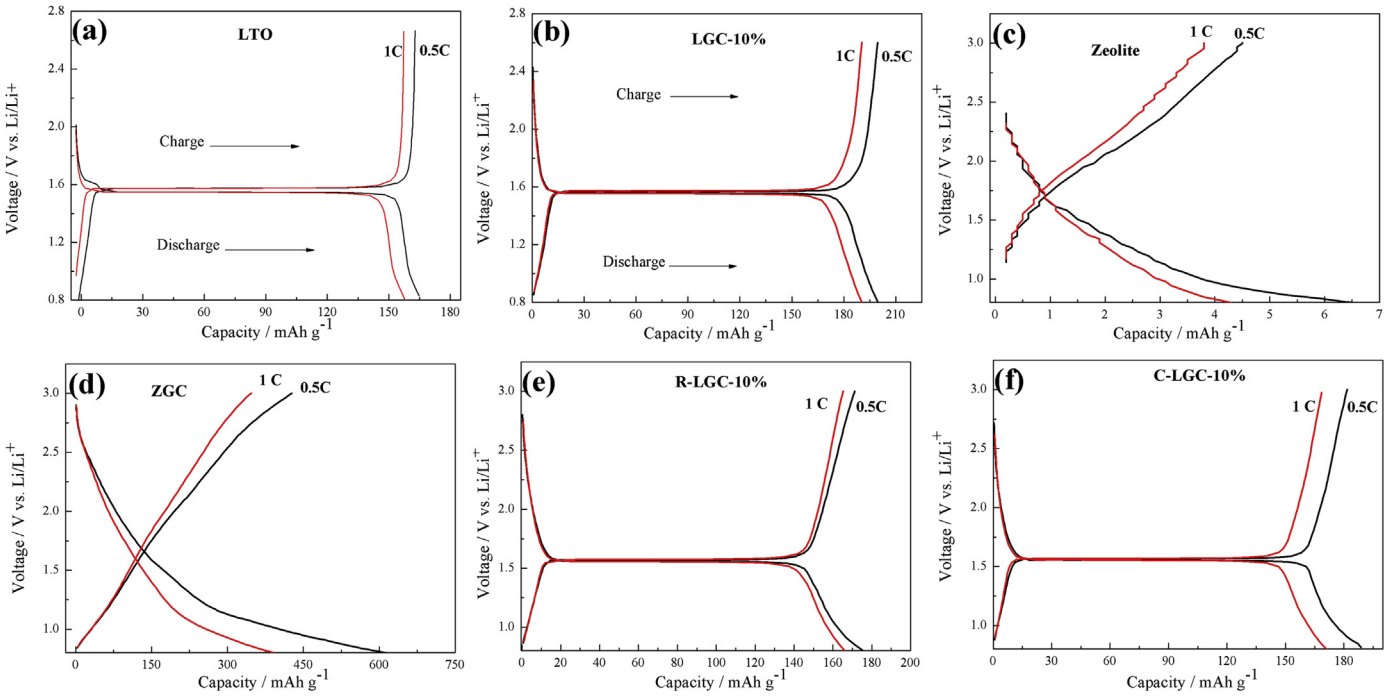

Fig. 6. Discharge/charge curves of (a) LTO, (b) LGC-10%, (c) zeolite, (d) ZGC, (e) R-LGC-10% and (f) C-LGC-10% electrodes at 0.5C and 1C, respectively.

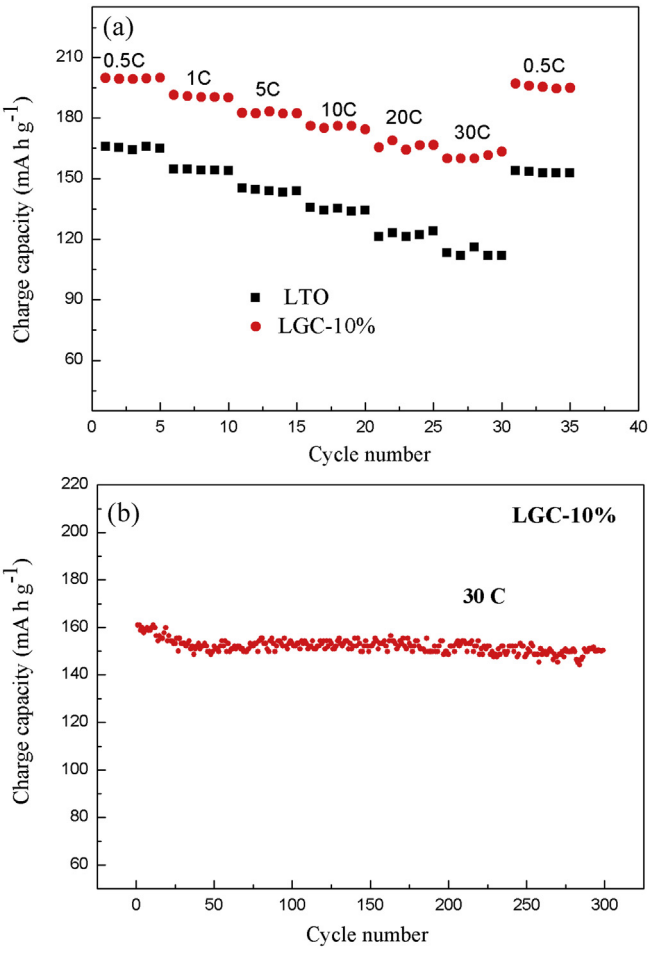

Fig. 7. (a) Rate capabilities of the LTO and LGC-10% at different rates and (b) cyclic performance of the LGC-10% at 30C.

and a charge capacity of 162 mAh g^{-1} could be obtained even at the rate of 30C (Fig. 7a). However, at the same rate, the charge capacity is only 110 mAh g^{-1} for LTO. This excellent rate capability of the LGC-10% electrode can be explained mainly by the reduced GO [20] or/and CMC binder-free. In order to verify which one plays a major role, the LTO/CMC/GO/S–P (80:10:5:5) composition electrode (nominated as LGCC-1) has been added to compare with the performance of the LTO and LGC-10%, and the results reveal that the good performance of LGC-10% compared to LTO is considered to be mainly attributed to CMC binder-free (Fig. S3 of Supplementary materials).

The relation between the discharge/charge specific capacity and the number of cycles of the LGC-10% at 30C is shown in Fig. 7b, which displays good cyclic performance of this electrode. In the first cycle, the charge capacity is 160 mAh g^{-1} at 30C, and after 300 discharge/charge cycles, it still remains at 156 mAh g^{-1}, a 97.5%

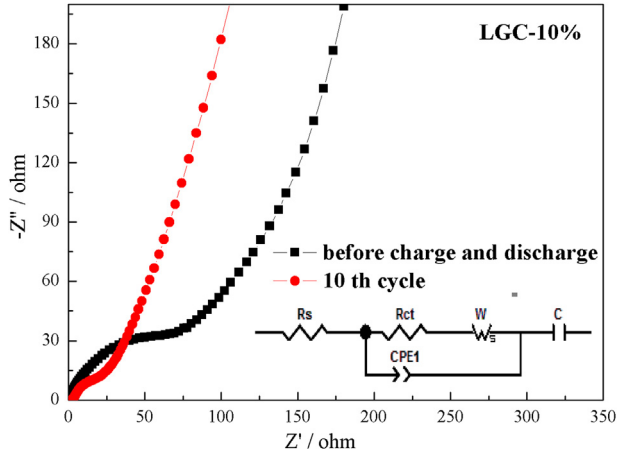

Fig. 8. AC impedance spectra of before and the after 10th cycle of LGC-10% electrode with the equivalent circuit from the EIS measurements (inset).

retention of the first charge capacity, which may be attributed to the stable cycle life of GO as reported earlier [28,29].

In order to further verify the idea that reduced GO after the first discharge process can improve the rate capability of the LGC-10%, EIS test is implemented. Fig. 8 shows the EIS of the LGC-10% electrode before and after 10th cycle discharge/charge processes. These AC impedance spectra are fitted by Z-View software [30] and shown in the inset of Fig. 8 and Table 2. Here R_s is the resistance of the electrolyte, R_{ct} the charge transfer resistance at the particle/electrolyte interface, and W the Warburg impedance, represents the Li-ion diffusion process, constant phase element (CPE) represents the double-layer capacitance and C is the insertion capacitance at the applied potential. From Table 2, the R_{ct} of LGC-10% electrode is 74 Ω before cycling, and decreases to 32 Ω after discharge/charge processes. This finding could prove that the electrochemical reduction of oxygen groups on the surface of graphene oxide sheets during the discharge/charge process, which increases the electric conductivity of the LGC-10% electrode [31].

Shown in Fig. 9a are the CV within a potential window of 0.8–3.0 V (vs. Li/Li^+). It is widely known that a sharp and well-resolved peak generally signifies fast Li^+ insertion/deinsertion, whereas a broad peak suggests a sluggish process. From the CV comparison shown in Fig. 9a, it can be seen that the CV curves of LTO are broadening with the increase of scan rate, while those of the LGC-10% retain a stable similar shape. In addition, the peak potential difference between anodes and cathodes of LGC-10% is smaller than that of LTO, which indicates the LGC-10% has smaller polarization and better rate capability. The relation between peak currents and scan rates can indicate the electrochemical reaction characteristics [32,33]. For the diffusion-limited process, the peak current is proportional to the square roots of the scan rate ($v^{1/2}$) as the following Randles–Sevcik equation [34]:

$$i_p = 2.69 \times 10^5 n^{3/2} D^{1/2} C v^{1/2}$$

where D is the diffusion coefficient, C is concentration of the reactant and n represents the number of transfer electrons. Linear correlation between peak currents and the square roots of the scan rate in the anodic process can be observed from both LTO and LGC-10%, as shown in Fig. 9b, which signifies obvious diffusion-controlled electrode process. Furthermore, the slope of the fitted line is dependent on the diffusion coefficient in the equation about the peak current and scan rate. Therefore it can be deduced that the LGC-10% has higher diffusion coefficient by the comparison of the slopes of these two straight lines. Compared with the two electrodes, the GO or/and CMC binder-free may effectively improve the electrochemical reaction kinetics of Li^+ insertion/deinsertion. To verify which one play a major role in improving the diffusion coefficient, the other two electrodes, LGCC-1 and LGCC-2, were investigated and the results reveal that the improvement of the electrochemical reaction kinetics of LGC-10% is considered to be mainly attributed to CMC binder-free (Fig. S4 of Supplementary materials).

However, the LGC-10% electrode notably exhibits poor initial coulombic efficiency (the percentage ratio of discharge-to-charge capacity) of only 80% under a current rate of 0.5C (Fig. S5 of Supplementary materials). The Li-ion irreversible consumption may come from certain side reactions, such as the electrochemical reduction of oxygen-containing functional groups in the LGC-10% [20]. To improve the coulombic efficiency of the as-prepared LGC-10% anode material, a variety of approaches have been explored, such as electric plating and mild pre-reduction. The results of these explorations are to be collected and reported in near future.

Table 2
Fitted parameters of equivalent circuit of Fig. 8.

Electrodes	R_s (Ω)	R_{ct} (Ω)
LGC-10% (before discharge and charge)	3.5	74
LGC-10% (after10th cycle)	2.6	32

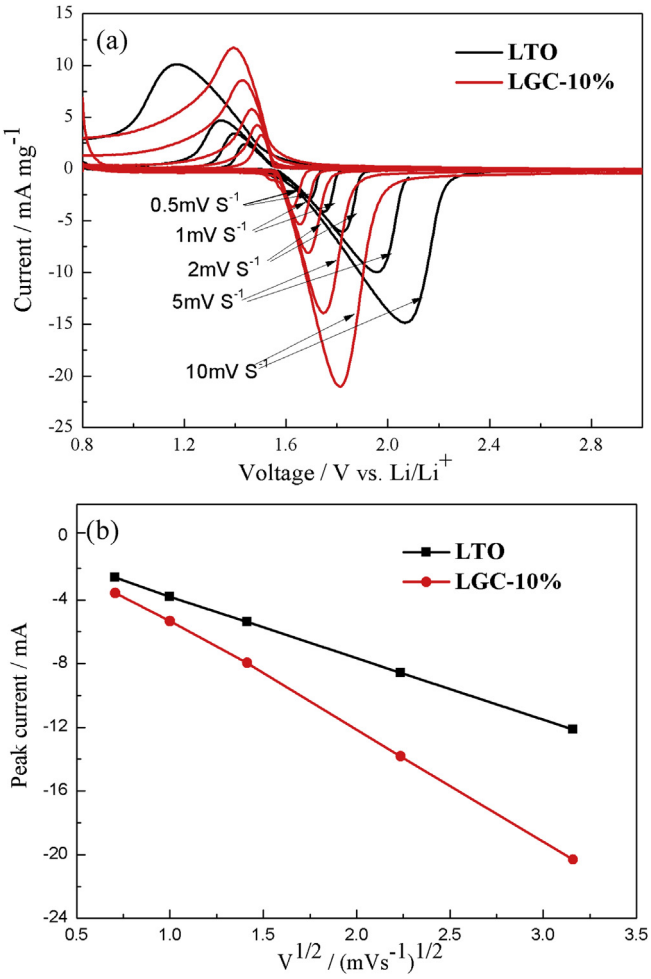

Fig. 9. (a) Cyclic voltammograms of the LTO and LGC-10% electrodes and (b) the cathodic peak currents against square roots of scan rate for the two electrodes.

4. Conclusions

The LGC-10% electrode by incorporating LTO particles and GO nanosheets is prepared, which exhibits obviously improved specific capacity and rate capability compared with the pure LTO. 10 wt% GO in the LGC-10% composite not only effectively increases the specific capacity, but also plays the role of polymer binder. Meanwhile, the composite with CMC binder-free, could improve the ability of lithium ion diffusion, thus improves the rate capability of the LGC-10% composite. This excellent electrochemical performance makes LGC-10% a promising anode material for large capacity and high rate Li-ion batteries and this simple preparation method enables its production on a large scale.

Acknowledgements

This work was carried out with financial support from MOST of China (2011CB932604). Also we are grateful for the help of Analytical and Testing Center of Chengdu Branch, Chinese Academy of Sciences.

Appendix A. Supplementary data

Supplementary data related to this article can be found at http://dx.doi.org/10.1016/j.jpowsour.2014.09.154.

References

[1] M. Imazaki, L.N. Wang, T. Kawai, K. Ariyoshi, T. Ohzuku, Electrochim. Acta 56 (2011) 4576–4580.
[2] N. Takami, H. Inagaki, Y. Tatebayashi, H. Saruwatari, K. Honda, S. Egusa, J. Power Sources 244 (2013) 469–475.
[3] W.W. Lee, J.M. Lee, J. Mater. Chem. A 2 (2014) 1589–1626.
[4] K. Amine, I. Belharouak, Z.H. Chen, T. Tran, H. Yumoto, N. Ota, S.T. Myung, Y.K. Sun, Adv. Mater. 22 (2010) 3052–3057.
[5] B.H. Li, C.P. Han, Y.B. He, C. Yang, H.D. Du, Q.H. Yang, F.Y. Kang, Energy Environ. Sci. 5 (2012) 9595–9602.
[6] E.M. Sorensen, S.J. Barry, H.K. Jung, J.R. Rondinelli, J.T. Vaughey, K.R. Poeppelmeier, Chem. Mater. 18 (2006) 482–489.
[7] L. Kavan, M. Gratzel, Electrochem. Solid-State Lett. 5 (2002) A39–A42.
[8] D. Bresser, E. Paillard, M. Copley, P. Bishop, M. Winter, S. Passerini, J. Power Sources 219 (2012) 217–222.
[9] C. Jiang, M. Ichihara, I. Honma, H.S. Zhou, Electrochim. Acta 52 (2007) 6470–6475.
[10] M.D. Ji, Y.L. Xu, Z. Zhao, H. Zhang, D. Liu, C.J. Zhao, X.Z. Qian, C.H. Zhao, J. Power Sources 263 (2014) 296–303.
[11] C.C. Yang, H.C. Hu, S.J. Lin, W.C. Chien, J. Power Sources 258 (2014) 424–433.
[12] Y.Y. Zhang, C.M. Zhang, Y. Lin, D.B. Xiong, D. Wang, X.Y. Wu, D.N. He, J. Power Sources 250 (2014) 50–57.
[13] J. Wolfenstine, J.L. Allen, J. Power Sources 180 (2008) 582–585.
[14] G.J. Wang, J. Gao, L.J. Fu, N.H. Zhao, Y.P. Wu, T. Takamura, J. Power Sources 174 (2007) 1109–1112.
[15] Y.R. Jhan, J.G. Duh, J. Power Sources 198 (2012) 294–297.
[16] H.S. Li, L.F. Shen, X.G. Zhang, J. Wang, P. Nie, Q. Che, B. Ding, J. Power Sources 221 (2013) 122–127.
[17] L. Cheng, J. Yan, G.N. Zhu, J.Y. Luo, C.X. Wang, Y.Y. Xia, J. Mater. Chem. 20 (2010) 595–602.
[18] J. Gao, J.R. Ying, C.Y. Jiang, C.R. Wan, J. Power Sources 166 (2007) 255–259.
[19] J.X. Zhang, H.Q. Cao, X.L. Tang, W.F. Fan, G.C. Peng, M.Z. Qu, J. Power Sources 241 (2013) 619–626.
[20] J.X. Zhang, Z.W. Xie, W. Li, S.Q. Dong, M.Z. Qu, Carbon 74 (2014) 153–162.
[21] W.S. Hummers, R.E. Offeman, J. Am. Chem. Soc. 80 (1958), 1339–1339.
[22] N.I. Kovtyukhova, P.J. Ollivier, B.R. Martin, T.E. Mallouk, S.A. Chizhik, E.V. Buzaneva, A.D. Gorchinskiy, Chem. Mater. 11 (1999) 771–778.
[23] X. Guo, H.F. Xiang, T.P. Zhou, X.K. Ju, Y.C. Wu, Electrochim. Acta 130 (2014) 470–476.
[24] Y. Shi, L. Wen, F. Li, H.M. Cheng, J. Power Sources 196 (2011) 8610–8617.
[25] Q. Zhang, W.J. Peng, Z.X. Wang, X.H. Li, X.H. Xiong, H.J. Guo, Z.G. Wang, F.X. Wu, Solid State Ionics 236 (2013) 30–36.
[26] S.W. Lee, N. Yabuuchi, B.M. Gallant, S. Chen, B.S. Kim, P.T. Hammond, Y. Shao-Horn, Nat. Nanotechnol. 5 (2010) 531–537.
[27] E. Peled, C. Menachem, D. Bar-Tow, A. Melman, J. Electrochem Soc. 143 (1996) L4–L7.
[28] H.H. Zhou, G.Y. Han, Y.M. Xiao, Y.Z. Chang, H.J. Zhai, J. Power Sources 263 (2014) 259–267.
[29] I.M.D. Salas, Y.N. Sudhakar, M. Selvakumar, Appl. Surf. Sci. 296 (2014) 195–203.
[30] Z.W. Xie, P. He, L.C. Du, F.Q. Dong, K. Dai, T.H. Zhang, Electrochim. Acta 88 (2013) 390–394.
[31] J. Giraudet, M. Dubois, J. Inacio, A. Hamwi, Carbon 41 (2003) 453–463.
[32] C. Lai, Y.Y. Dou, X. Li, X.P. Gao, J. Power Sources 195 (2010) 3676–3679.
[33] X.J. Wang, L. Wang, J.J. Wang, T. Chen, J. Phys. Chem. B 108 (2004) 5627–5633.
[34] A.J. Bard, L.R. Faulkner, Electrochemical Methods: Fundamentals and Application, Wiley, 2000.